



# Influenza A Virus-Driven Airway Inflammation may be Dissociated From Limb Muscle Atrophy in Cigarette Smoke-Exposed Mice

Kevin Mou, Stanley M. H. Chan, Kurt Brassington, Aleksandar Dobric, Simone N. De Luca, Huei Jiunn Seow, Stavros Selemidis, Steven Bozinovski and Ross Vlahos\*

School of Health and Biomedical Sciences, RMIT University, Melbourne, VIC, Australia

## OPEN ACCESS

### Edited by:

Isaac Kirubakaran Sundar,  
University of Kansas Medical Center,  
United States

### Reviewed by:

Rong Hai,  
University of California, Riverside,  
United States

Brian Gregory George Oliver,  
University of Technology Sydney,  
Australia

Graeme Zosky,  
University of Tasmania, Australia

Thomas H. Thatcher,  
Virginia Commonwealth University,  
United States

### \*Correspondence:

Ross Vlahos  
ross.vlahos@rmit.edu.au

### Specialty section:

This article was submitted to  
Respiratory Pharmacology,  
a section of the journal  
Frontiers in Pharmacology

**Received:** 21 January 2022

**Accepted:** 17 February 2022

**Published:** 18 March 2022

### Citation:

Mou K, Chan SMH, Brassington K,  
Dobric A, De Luca SN, Seow HJ,  
Selemidis S, Bozinovski S and Vlahos R  
(2022) Influenza A Virus-Driven Airway  
Inflammation may be Dissociated From  
Limb Muscle Atrophy in Cigarette  
Smoke-Exposed Mice.  
*Front. Pharmacol.* 13:859146.  
doi: 10.3389/fphar.2022.859146

Limb muscle dysfunction is a hallmark of Chronic Obstructive Pulmonary Disease (COPD) which is further worsened following a viral-induced acute exacerbation of COPD (AECOPD). An amplified airway inflammation underlies the aggravated respiratory symptoms seen during AECOPD, however, its contributory role to limb muscle dysfunction is unclear. The present study examined the impact of influenza A virus (IAV)-induced exacerbation on hind limb muscle parameters. Airway inflammation was established in male BALB/c mice by exposure to cigarette smoke (CS) for 8 weeks. Exacerbation was then induced via inoculation with IAV, and various lung and muscle parameters were assessed on day 3 (peak of airway inflammation) and day 10 (resolution phase) post-infection. IAV infection exacerbated CS-induced airway inflammation as evidenced by further increases in immune cell counts within bronchoalveolar lavage fluid. Despite no significant impact on muscle mass, IAV exacerbation worsened the force-generating capacity of the tibialis anterior (TA) muscle. Protein oxidation and myogenic disruption was observed in the TA following CS exposure, however, IAV exacerbation did not augment these detrimental processes. To further explore the contributory role of airway inflammation on myogenic signaling, cultured myotubes were exposed to conditioned medium (CM) derived from bronchial epithelial cells stimulated with polyinosinic:polycytidylic acid and cigarette smoke extract (CSE). Despite an amplified inflammatory response in the lung epithelial cells, the CM derived from these cells did not potentiate myogenic disruption in the C2C12 myotubes. In conclusion, our data suggest that certain parameters of limb muscle dysfunction seen during viral-induced AECOPD may be independent of airway inflammation.

**Keywords:** viral exacerbation, COPD, muscle weakness, fiber type transformation, lung-to-muscle axis, myogenic disruption, conditioned medium

## INTRODUCTION

Chronic obstructive pulmonary disease (COPD) is a heterogenous, incurable inflammatory disorder associated with exposure to noxious particles or gases, with the leading causative factor being cigarette smoking (CS) (Barnes, 2018). The disease is characterized by persistent airflow limitation, and the combination of small airway disease and parenchymal destruction that are progressive in

nature (Decramer and Janssens, 2013). Recent studies have shown that COPD is a complex disease with both pulmonary and extrapulmonary manifestations (Vanfleteren et al., 2016). Skeletal muscle dysfunction is an important extrapulmonary comorbidity of COPD (Decramer and Janssens, 2013; Passey et al., 2016) and causes a rapid decline in the quality of life, and premature death (Gosselink et al., 1996; Marquis et al., 2002). People with COPD often experience acute deterioration of respiratory symptoms (e.g., cough, sputum production, and dyspnea), known as acute exacerbation of COPD (AECOPD) (Gosker et al., 2021). Although AECOPD may be caused by different etiological factors including those of a non-infectious nature, respiratory viruses are identified in 30–50% of all AECOPD episodes (Mathioudakis et al., 2020), in which 25% of these cases are primarily caused by influenza A virus (IAV) (Mackay and Hurst, 2013). In addition to the diagnostic respiratory symptoms, heightened pulmonary inflammation is a key pathological feature of viral AECOPD, driven by a combination of excessive proinflammatory cytokine/chemokine production (IL-6, IL-8, TNF- $\alpha$ , IFN- $\gamma$ , GM-CSF), excessive oxidative stress, and protease-antiprotease imbalances (Barnes, 2017). The recruitment of inflammatory cells such as neutrophils, into the lungs further increases the secretion of proinflammatory factors, superoxide production, and protease release, resulting in the amplification of lung inflammation and destruction of airway structures (Barnes, 2018). Consequently, the presence of respiratory viruses during an exacerbation of COPD has been correlated to worsened symptoms and a delayed recovery (Mathioudakis et al., 2020).

The term “muscle dysfunction” encompasses the loss of force generating capacity (i.e., strength), loss of mass, and increase in fatigability of a muscle. These are commonly observed in the limb muscles of COPD patients (Vogelmeier et al., 2017) and of note, are predominantly seen in the lower limbs (Gosselink et al., 1996; Bernard et al., 1998). The preferential impact on the lower limbs may be related to a greater reduction in activity of these muscles in people with COPD (Maltais et al., 2014), together with the weight bearing nature of the lower limb muscles. During AECOPD, muscle strength, mass, and fatigability are found to be further impaired, which may lead to a longer duration of hospitalization and readmission within the following 3 months (Girón et al., 2009). Moreover, exacerbation-linked muscle dysfunction has been demonstrated to be an independent predictor of future hospitalization for COPD patients (Schols et al., 2005; Amado et al., 2019). Because of this, attempts have been made to retain/restore muscle mass in these patients with androgenic anabolic steroids. Despite the short-term benefits on lean body mass and muscle size, there were no consistent effects on muscle strength, exercise capacity, or pulmonary function (Pan et al., 2014). Moreover, long-term use of anabolic steroids was found to be associated with a number of adverse effect such as insulin resistance, cardiovascular disease, hepatotoxicity and hormonal imbalance effects (Pan et al., 2014). Therefore, it is of importance to understand the key mechanisms responsible for the further deterioration of muscle dysfunction in AECOPD.

A number of clinically relevant risk factors are believed to contribute to muscle dysfunction in AECOPD, including physical

inactivity, malnutrition, therapeutic interventions (e.g., anti-inflammatory steroids) and the “spill-over” of airway inflammatory mediators into the systemic circulation (Barnes and Celli, 2009; Bernardo et al., 2015). It has been postulated that airway inflammation alone is sufficient to cause muscle dysfunction (Files et al., 2012), and furthermore, attenuation of airway inflammation by noninvasive mechanical ventilation reduces systemic inflammation during AECOPD (Hillas et al., 2016). This raises an important observation that airway inflammation may be directly linked to the further deterioration of muscle dysfunction seen in AECOPD, particularly when IAV infection has been shown to exacerbate airway inflammation (Bozinovski et al., 2012; Wang et al., 2019). The present study aimed to investigate the effect of IAV infection-driven airway inflammation on skeletal muscle dysfunction in the presence or absence of CS, by utilising a well-established preclinical model of AECOPD (Vlahos and Bozinovski, 2014) and a novel conditioned medium (CM) *in vitro* approach (Mohammadipoor et al., 2018).

## MATERIALS AND METHODS

### Animals

Because of the strain dependence on the development of respiratory disease following cigarette smoke (CS) exposure (Vlahos et al., 2006), male Balb/C mice were chosen for this experiment. 7-week-old male BALB/c mice were obtained from the Animal Resources Centre Pty. Ltd. (Perth, WA, Australia) and allowed to acclimatize for 1 week at the RMIT Animal Facility (Bundoora, VIC, Australia). Mice were housed in micro-isolator cages with an ambient temperature of 21°C under a 12:12 light/dark cycle (lights on at 7a.m. and off at 7p.m. AEST). Water and standard mouse chow were available *ad libitum*. Body weight was monitored 3 times a week. All experimental procedures and protocols were conducted in accordance with the Australian Code of Practice for the Care and Use of Animals for Scientific Purposes, and approved by the RMIT University Animal Ethics Committee (AEC 1533).

### Influenza A Virus Amplification

Mem71 (H3N1) is a strain of IAV with intermediate virulence, which is a result of genetic reassortant of A/Memphis/1/71 (H3N2)  $\times$  A/Bellamy/42 (H1N1) (Reading et al., 1997; Gualano et al., 2008). The virus was grown in Madin-Darby canine kidney (MDCK) cells, which were maintained at 37°C/5% CO<sub>2</sub> in RPMI 1640 medium containing 2 mM L-glutamine, 2 mM sodium pyruvate, 30  $\mu$ g/ml gentamycin, 100 I.U./ml penicillin, 100  $\mu$ g/ml streptomycin and 10% v/v heat inactivated FCS (Thermo Fisher Scientific, Massachusetts, United States). For viral amplification, 90% confluent MDCK cells were washed twice in PBS and infected with egg grown virus at 0.01 plaque forming units/cell. After 1.5 h, the inoculum was removed, cells were washed twice with PBS, followed by the addition of a low protein, serum free medium (VP-SFM, Thermo Fisher Scientific, Massachusetts, United States) containing 0.5  $\mu$ g/ml trypsin. Virus was harvested 48 h later, when there was

extensive viral cytopathic effect. Flasks were shaken to loosen cells, the medium and cells were collected, briefly vortexed, subjected to a low-speed clearing spin and the clarified supernatant was collected and stored in aliquots at  $-80^{\circ}\text{C}$  until required.

## Cigarette Smoke Exposure and Influenza A Virus Infection

Mice were placed in 18L Perspex containers in a standard fume hood and exposed to smoke generated from three cigarettes (Winfield Red, Phillip Morris, VIC, Australia; the average particulate matter was  $419\text{ mg/m}^3$ ) over a 1-h period. CS was generated in 60 ml tidal volumes over a 10 s period in order to mimic the inhalation rates observed in human smokers. Mice were exposed to CS in this fashion 3 times a day (15 min per cigarette), with a 2-h break between smoke sessions (9 cigarettes per day total). CS exposure occurred for 5 days a week for 8 weeks. Control animals (Sham) were also placed in 18L Perspex containers but were not exposed to CS. At the end of 8 weeks of CS exposure, mice were anesthetized with methoxyflurane (Medical Developments International, VIC, Australia) and intranasally inoculated with either sterile phosphate buffered saline (PBS; diluent) or influenza A virus (Mem71/H3N1 strain at  $1 \times 10^{4.5}$  plaque forming units) dissolved in PBS. Following infection, CS exposure was ceased and mice were monitored periodically until the end of experiment for signs of distress (slowed respiration, reduced activity) and culled if symptoms persisted.

## Locomotor Activity Assessment

One day prior to termination, the locomotor activity of the mice was assessed in an open field arena. Locomotor activity was assessed between 8 a.m. and 1 p.m. to limit potential impacts of circadian rhythm. Mice were placed in the center of an empty  $60\text{ cm} \times 60\text{ cm} \times 60\text{ cm}$  black plywood box and allowed to freely explore the environment for 8 min. The open field arena was cleaned with 70% ethanol prior to use and before each subsequent animal tested. The activity of the mice was filmed with a camcorder positioned above the arena (Panasonic HC-W585M, Osaka, Japan) and later scored on Ethovision XT software (v11.5; Noldus Information Technology, Wageningen, Netherlands). Briefly, a single zone was created in Ethovision that corresponded with the entire box. Mice were scored for total distance travelled within the zone during an 8-min period and trace maps were generated.

## Muscle Function Testing

At the end of the protocol, mice were anesthetized with a mixture of ketamine (80 mg/kg)/xylazine (16 mg/kg) and incisions were made to expose the tibialis anterior (TA) muscle, with care taken to avoid cutting the fascia as previously described (Chan et al., 2021). Briefly, the distal tendon was separated from the surrounding fascia in order to free the tendon from the ankle joint. The mouse was transferred to a heated platform ( $37^{\circ}\text{C}$ ) attached to an *in situ* contractile apparatus (1300A Aurora 3-in-1 whole animal system; Aurora Scientific, Ontario, Canada) and the

limb of interest was secured to the platform via a foot clamp and a needle inserted through the patellar tendon and into the platform. The separated tendon was tied and secured to an isometric force transducer via suture threads. Two fine electrodes were inserted into the muscle belly  $\sim 3\text{--}5\text{ mm}$  apart and penetrating just below the surface of the muscle. The muscle was periodically bathed with warm saline to prevent drying.

The TA was stimulated twice with a sustained contraction at 100 Hz with a 2-min rest interval in between, in order to settle the muscle and tighten the knots. Optimal muscle length ( $L_0$ ) was determined by increasing the length of the muscle with a micromanipulator. The muscle was stimulated with twitch contractions (single action potential allowing contraction then relaxation) every 30 s until a repeatable maximum peak twitch force was obtained.  $L_0$  was measured using precision digital calipers as the distance between the distal myotendinous junction and the insertion of the TA at the base of the knee. A force frequency test was performed which involved contractions induced at increasing frequencies (10, 20, 30, 50, 80, 100, 150, 200, 250, and 300 Hz) at 2-min intervals. Forces were converted to a digital signal and recorded by DYNAMIC MUSCLE ANALYSIS 611ATM (Aurora Scientific).

## Tissue Sample Collection

Mice were euthanized with sodium pentobarbitone (240 mg/kg; Virbac Australia, NSW, Australia) *via* intraperitoneal injection. Bronchoalveolar lavage fluid (BALF) was collected by flushing out the lungs with 400  $\mu\text{L}$  ice-cold PBS followed by three aliquots of 300  $\mu\text{L}$  ice-cold PBS, generating  $\sim 1\text{ ml}$  of BALF per mouse. The total number of viable cells in the BALF was measured by diluting 50  $\mu\text{L}$  of BALF with 50  $\mu\text{L}$  of an acridine orange stain (Invitrogen, VIC, Australia). Cells were counted on a standard Neubauer hemocytometer under fluorescent light with an Olympus BX53 microscope (Olympus, Tokyo, Japan). To differentiate between the cell populations in the BALF, 50,000 cells were centrifuged using  $\sim 50\text{--}200\text{ }\mu\text{L}$  of BALF at 400rpm for 10 min on a Shandon Cytospin 3 (Thermo Fisher Scientific, Massachusetts, United States). Dried cytopots were fixed with Shandon<sup>TM</sup> Kwik-Diff<sup>TM</sup> fixative (Thermo Fisher Scientific, Massachusetts, United States) and stained with Hemacolor Rapid Red and Blue dye (Merck, Australia). Cells were identified and differentiated into macrophages, lymphocytes, and neutrophils according to standard morphological criteria, with a minimum of 500 cells counted per slide. Hind limb muscles (quadriceps, TA, calf muscles) were dissected from each mouse, weighed, snap frozen in liquid nitrogen, and stored at  $-80^{\circ}\text{C}$  until required. Muscles for morphological analysis were frozen in Tissue-Tek O.C.T compound (ProSciTech, QLD, Australia) under liquid nitrogen cooled isopentane, then stored at  $-80^{\circ}\text{C}$  until required.

## Immunohistochemical Analyses

Frozen O.C.T embedded muscles were sectioned in a cryostat (Leica Biosystems, United States) for immunofluorescent staining of slow skeletal muscle myosin heavy chain (SM1; Santa Cruz Biotechnology Inc., TA, United States) and laminin (Novus Biologicals, Colorado, United States), as previously described (Chan et al., 2020) with slight modifications. Briefly, sections

were fixed in 4% paraformaldehyde in 0.1 M phosphate buffer for 10 min at room temperature. Slides were then rinsed with 1X PBS +0.1% Tween<sup>®</sup> 20 (PBST) and incubated with blocking buffer (5% fetal bovine serum, 0.5% Triton-X, 0.01% sodium azide, 1X PBS) for 2 h at room temperature. Fluorophore conjugated antibodies for SM1 and laminin were added to sections and allowed to incubate overnight at 4°C. Myofiber cross-sectional area was determined by staining sections for laminin. Muscle fiber typing was determined by staining muscle sections for SM1. Following overnight incubation, sections were washed with 1X PBST and slides were mounted with Fluoromount-G<sup>™</sup> Mounting Medium, with DAPI (Thermo Fisher Scientific, Massachusetts, United States) and cover slipped.

Slides were viewed and imaged using an Olympus Slide Scanner (VS120-S5, Olympus, United States) and analyzed using cellSens<sup>™</sup> Life Science Imaging Software (Olympus, United States). Briefly, user defined boundaries consistent across each sample (size and location) were created and the cross-sectional area of fibers within boundaries was measured using the cellSens<sup>™</sup> measuring tool. Fiber types were identified based on the staining color and oxidative myofibers were manually counted and expressed as a percentage of all fibers within boundaries.

### Cell Culture and Conditioned Media Study

Human bronchial epithelial cell line, BEAS-2B (CRL-9609; American Type Culture Collection, United States), were grown as monolayers in a humidified incubator with 5% CO<sub>2</sub> at 37°C in LHC-9 medium (Thermo Fisher Scientific, Massachusetts, United States) supplemented with 50 µg/ml gentamycin and 10% fetal calf serum (Thermo Fisher Scientific, Massachusetts, United States), with medium changes every 2–3 days. C2C12 murine myoblasts (CRL-1772, American Type Culture Collection) were cultured in high glucose Dulbecco's Modified Eagle's Medium (DMEM; Thermo Fisher Scientific, Massachusetts, United States) supplemented with 1% penicillin/streptomycin (100 units/mL penicillin and 100 µg/ml streptomycin; Thermo Fisher Scientific, Massachusetts, United States) and 10% fetal bovine serum (FBS; Thermo Fisher Scientific, Massachusetts, United States). Cells were cultured in a T-75 flask and were passaged at 70–80% confluence. The flasks were kept in a humidified incubator at 37°C with 5% CO<sub>2</sub>. To induce differentiation, confluent monolayers of C2C12 myoblasts were switched to differentiation medium (DM) consist of high-glucose DMEM supplemented with 1% penicillin/streptomycin and 2% horse serum (Thermo Fisher Scientific, United States) and the DM was changed daily. All experiments were performed on day 6 when majority of myoblasts have transformed into mature myotubes.

Cigarette smoke extract (CSE) was generated as previously described (Chan et al., 2021) with slight modifications. Briefly, one cigarette (Winfield Red, Phillip Morris International, Australia) was bubbled through a 25 ml of pre-warmed experimental media at a rate of 3 ml/s to produce 100% CSE stock solution. The stock solution was sterile filtered and diluted to obtain desirable concentration for experimentation. For the

CM study, BEAS-2B cells were stimulated with either polyinosinic:polycytidylic acid (poly I:C, 4 µg ml<sup>-1</sup>), 25% CSE, or the combination of the two for 6 h. At the end of the stimulation, the media from the respective conditions were harvested and centrifuged at 400 g, 5 min at 4°C. The supernatants representing the CM were transferred onto differentiated C2C12 myotubes for 18 h.

### Quantitative Real-Time PCR

Total RNA was extracted from muscle tissue and cells using the RNeasy<sup>®</sup> Mini Kit (Qiagen, Germany) according to manufacturer instructions. RNA was reverse transcribed to cDNA using the High-Capacity RNA-to-cDNA Kit (Thermo Fisher Scientific, Massachusetts, United States) according to manufacturer instructions and real time PCR reactions were performed on the QuantStudio 7<sup>™</sup> (Applied Biosciences, United States) using mouse specific TaqMan<sup>®</sup> Gene Expression Assays: *Igf-1b* (AIKALFT), *Mstn* (Mm01254559\_m1), *Cybb* (Mm01287743\_m1), *Gpx1* (Mm00656767\_g1), *Il-6* (Mm00443258\_m1), and *Tnfrα* (Mm00446190\_m1). All reactions were performed in triplicate and data obtained was normalized against glyceraldehyde 3-phosphate dehydrogenase (GAPDH), used as the reference gene, prior to analysis using the delta-delta Ct method.

### Western Blotting and Oxyblot

Tissue samples were homogenized in 500 µL of ice cold RIPA lysis buffer [150 mM NaCl, 1% Triton X-100, 0.5% Na-deoxycholate, 0.1% sodium dodecyl phosphate, 50 mM Tris (pH 8)] supplemented with β-mercaptoethanol (1%) and protease and phosphatase inhibitor cocktail (1%, Cell Signaling Technology, United States). The samples were incubated on ice for 30 min before being centrifuged for 10 min at 14,000 g at 4°C and supernatant was collected for immediate use or stored at -80°C. Protein concentrations were quantified through the use of a commercially available colorimetric bicinchoninic acid (BCA) protein assay kit (Thermo Fisher Scientific, Massachusetts, United States), following manufacturer instructions. For western blots, protein samples were denatured in SDS loading buffer (4x Laemmli buffer; 50 mM Tris-HCl pH 6.8, 2% SDS, 10% glycerol, 1% β-mercaptoethanol, 12.5 mM EDTA, 0.02% bromophenol blue). Western blot analyses were performed on 12% SDS PAGE gels to assess key signalling molecules including phospho-/pan- STAT1, phospho-/pan- JNK, GAPDH, BiP, phospho-/pan-eIF2α, phospho-/pan-p70S6 kinase, phospho-/pan- S6rp, phospho-/pan- 4E-BP1, tubulin (Cell Signaling Technology, United States), MAFbx and MURF-1 (Abcam, United States). For oxyblots, protein samples were derivatized and stabilized using the OxyBlot Protein Oxidation Detection kit (Merck, Massachusetts, United States) for immunoblot detection of carbonyl groups, following manufacturer instructions. Membranes were developed using chemiluminescent substrates and imaged using the ChemiDoc system (BioRad Laboratories Inc., United States). Quantitative densitometry analysis of bands of interest was performed using Image Lab software (Ver. 6.0, Bio-Rad Laboratories Inc.).

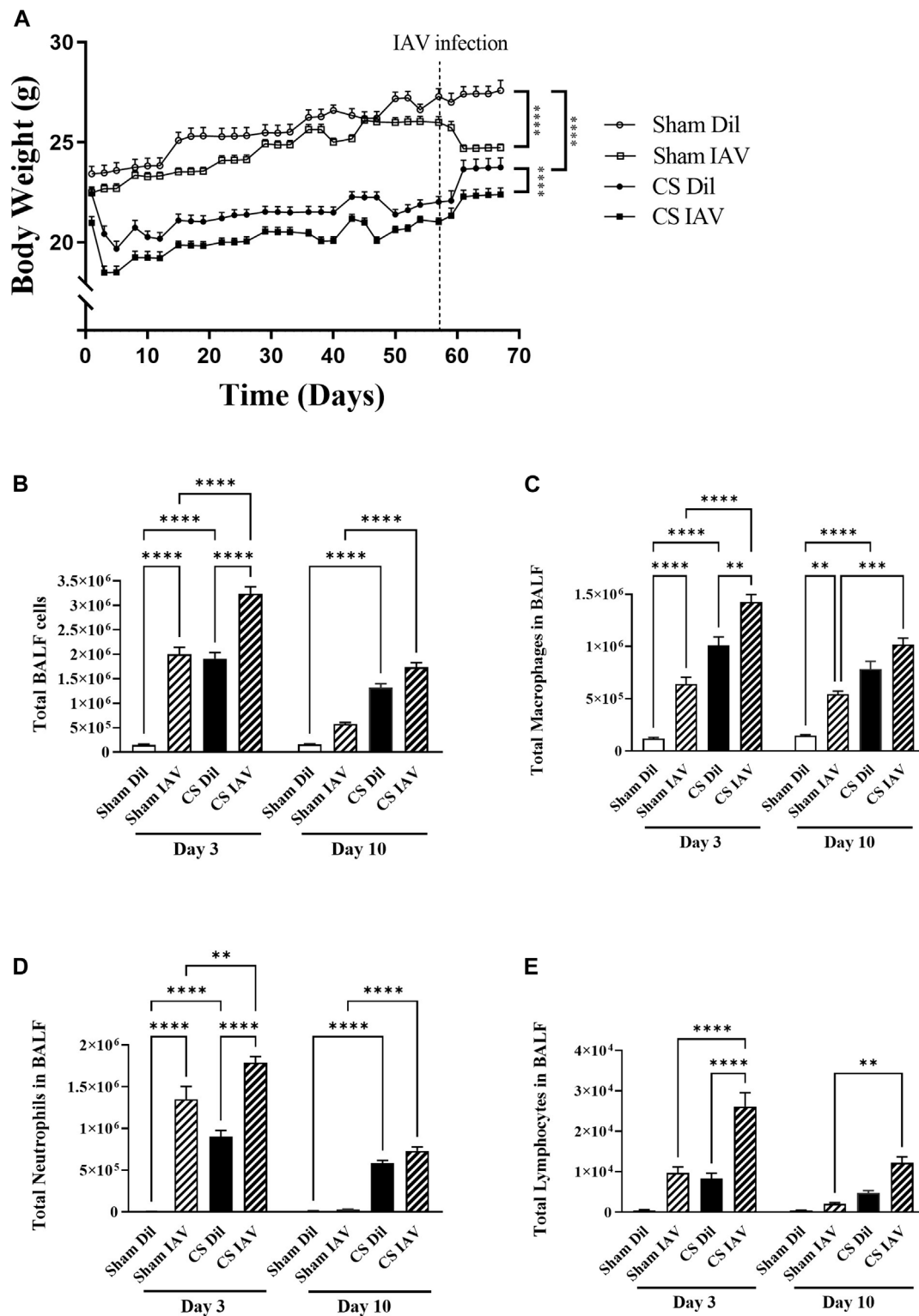


**FIGURE 1 |** Effect of CS exposure and influenza A virus (IAV) infection on body weight and BALF cellularity. **(A)** Progressive body weight of mice across the experiment, and number of **(B)** total cells, **(C)** macrophages, **(D)** neutrophils and **(E)** lymphocytes in the bronchoalveolar lavage fluid in CS-exposed and Sham mice following IAV infection. Data shown as mean +SEM (n = 7 per group). \*\*p < 0.01, \*\*\*p < 0.001, \*\*\*\*p < 0.0001.

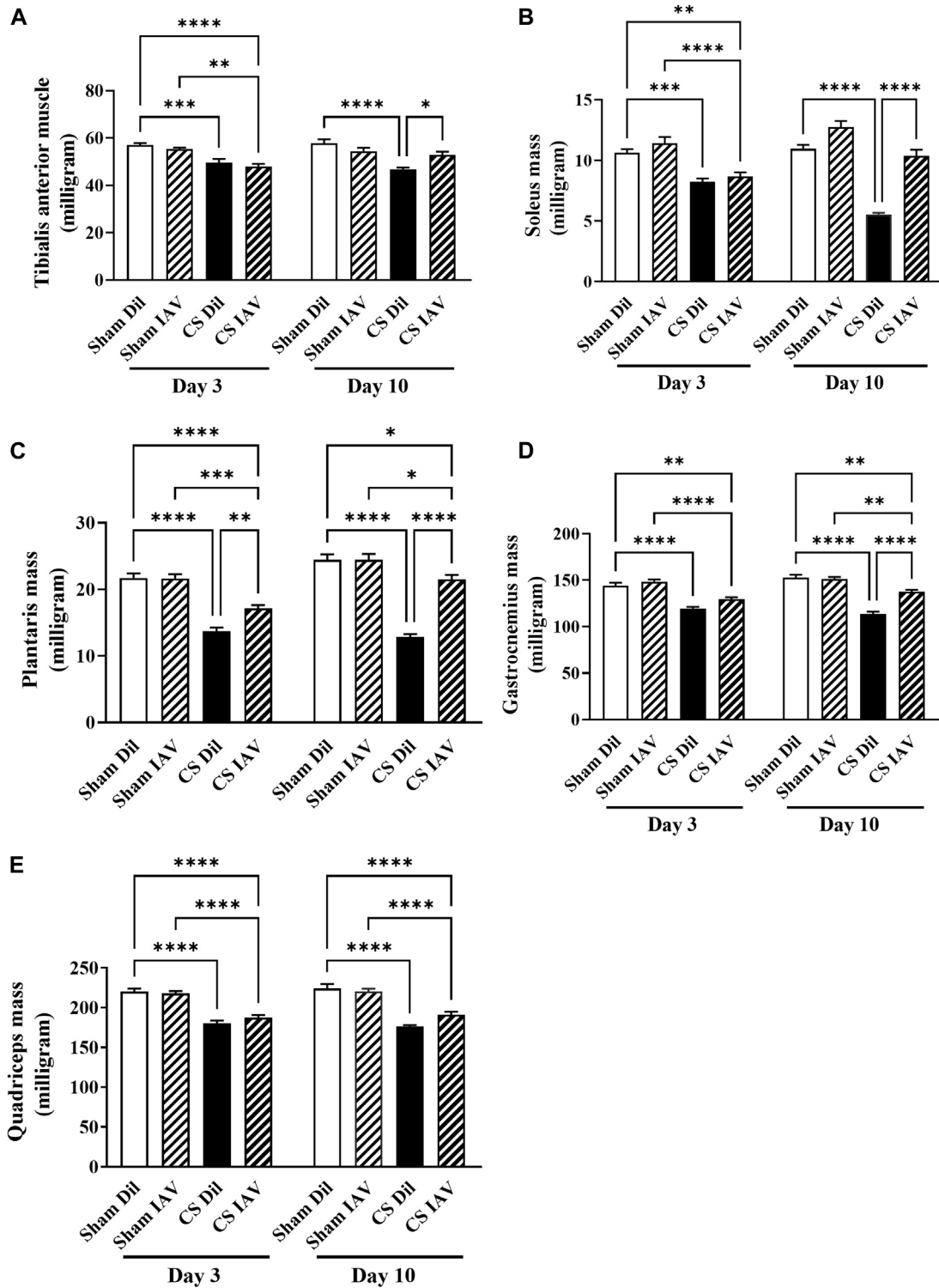


**FIGURE 2** | Effect of CS exposure and influenza A virus (IAV) infection on mass of hind limb muscles. The weight of the (A) tibialis anterior, (B) soleus, (C) plantaris, (D) gastrocnemius, and (E) quadriceps muscles from CS-exposed and Sham mice following IAV infection. Data shown as mean +SEM (n = 14 per group). \*p < 0.05, \*\*p < 0.01, \*\*\*p < 0.001, \*\*\*\*p < 0.0001.

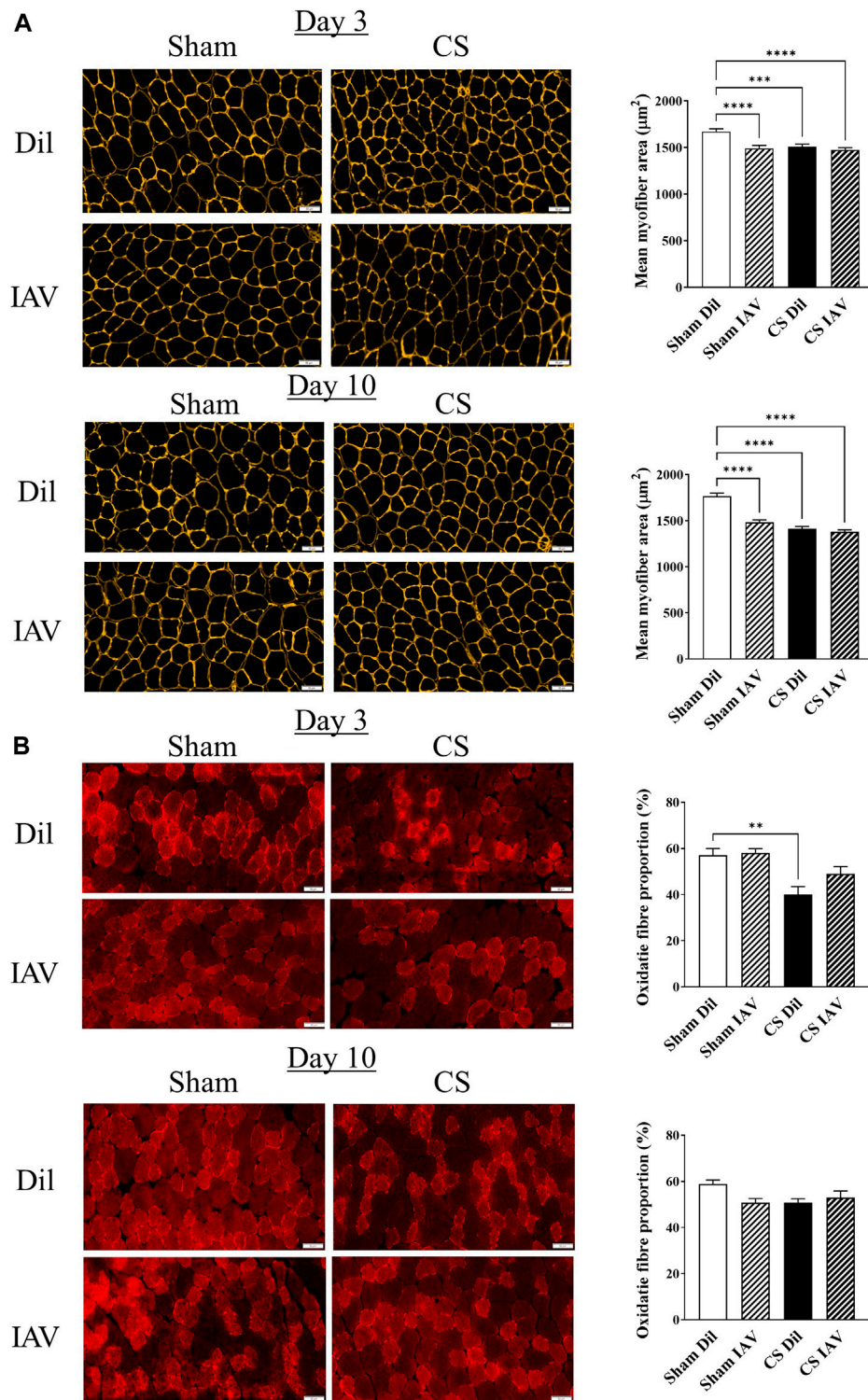


**FIGURE 3 |** Effect of CS exposure and influenza A virus (IAV) infection on morphology of tibialis anterior (TA) muscle. Immunofluorescent examination and quantitative data of **(A)** myofiber cross-sectional area with laminin staining and **(B)** fiber distribution with slow myosin heavy chain staining, in cross-sectioned TA of CS-exposed and/or IAV infected mice 3- and 10-days post infection. Scales bars: 50  $\mu\text{m}$ . At least 600 fibers were counted per animal. Data shown as mean +SEM ( $n = 5$  per group). \*\* $p < 0.01$ , \*\*\* $p < 0.001$ , \*\*\*\* $p < 0.0001$ .

## Statistical Analyses

All data are presented as mean  $\pm$  SEM unless otherwise stated;  $n$  represents the number of mice. Multivariate analysis was performed *via* two-way ANOVA, followed by Tukey *post hoc* test where significant differences were found. All statistical analyses were performed using PRISM 9<sup>TM</sup> (GraphPad Software, CA, United States). In all cases, statistical significance was assumed when  $p < 0.05$ .

## RESULTS

### IAV Infection Exacerbates Airway Inflammation Without Causing Skeletal Muscle Loss

CS exposure suppressed body weight gain ( $\sim 2$  g lower than Sham) which was maintained throughout the course of the experiment (**Figure 1A**). Following IAV infection, Sham mice experienced a  $\sim 9\%$  reduction in body weight compared to the non-infected Sham mice. Under CS condition, IAV infection also caused a similar reduction in body weight. CS exposure or IAV alone produced a robust increase in total cellularity within the BALF (**Figure 1B**). This was attributed to an increase in macrophage, neutrophil, and lymphocyte counts (at day 3). This was further augmented by the combination of CS exposure and IAV infection (**Figures 1B–E**) recapitulating that of AECOPD in human patients (Bozinovski et al., 2012; Wang et al., 2019). Similar to our previous observations (Oostwoud et al., 2016), the IAV infection-driven exacerbation was characterized by a peak in airway inflammation at day 3 that was resolved by day 10, marking the resolution phase of infection.

CS exposure caused a global reduction in mass of the hind limb muscles (**Figures 2A–E**), which was sustained throughout the course of the experiment. This was characterized by a 13 and 30% decrease in mass of the TA (**Figure 2A**) and plantaris (**Figure 2C**) respectively, which are predominated by fast-twitch fibers. Similar trends were observed in the slow-twitch fiber predominant soleus with a 22% decrease observed (**Figure 2B**), along with a 17% loss in both the mixed-fiber predominant gastrocnemius and quadriceps (**Figures 2D,E**). Despite the exacerbated airway inflammation, the combination of CS and IAV infection (at day 3) did not result in any further loss of muscle mass. By day 10, most of the muscle loss driven by the combination of CS exposure and IAV infection returned to Sham level (**Figures 2A–E**), suggesting viral exacerbation is unlikely to have additive effects on CS-induced muscle loss.

### IAV Infection Decreased Myofiber Area Irrespective of CS Exposure

In line with the loss of TA muscle mass, CS exposure also caused a  $\sim 10\%$  reduction in mean myofiber cross-sectional area (CSA), which persisted throughout the course of experiment (**Figure 3A**). Despite the seemingly unaffected muscle mass, IAV infection also resulted in a similar reduction in mean myofiber CSA, in the Sham group. However, the suppressive

effects of IAV infection on mean myofiber CSA did not appear to be alleviated on day 10, unlike that of muscle mass (**Figure 3A**). Furthermore, immunostaining detected a significant reduction in the proportion of oxidative muscle fibers following CS exposure, suggesting the presence of a slow-to-fast fiber type shift, like that seen in people with stable COPD (Gosker et al., 2007). In contrast, IAV infection did not significantly impact fiber type composition, irrespective of CS exposure or time after infection (**Figure 3B**), suggesting viral exacerbation is unlikely to contribute to fiber type transformation of limb muscle.

### IAV Infection Exacerbated CS-Induced Contractile Impairment Independent of Locomotor Activity

To investigate the impacts of viral exacerbation on limb muscle function, we performed detailed functional analysis on day 3, when airway inflammation was at its peak (**Figures 1B–E**). Our correlational analyses revealed that the loss of TA mass is directly correlated with the peak increase (i.e., day 3) in BALF neutrophilia (**Figure 4A**), which is a common characteristic of both stable COPD and AECOPD (Gompertz et al., 2001; Hoenderdos and Condcliffe, 2013). Although a similar correlative trend was observed on day 10, the  $R_2$  value was much lower (**Figure 4B**), suggesting the main effects of viral exacerbation on limb muscle are most likely to occur on day 3. Our muscle function analysis found that either IAV infection or CS exposure caused a significant reduction in contractile function of the TA muscle, which was further deteriorated when IAV infection was combined with CS exposure (**Figure 4C**). In line with this, the specific force analysis demonstrated a 41 and 36% decrease in contractile function by IAV infection and CS exposure respectively when compared to Sham animals, while a 52% decrease was observed when IAV infection was combined with CS exposure (**Figure 4D**), suggesting the manifestation of muscle weakness. As muscle weakness is closely linked to reduced physical activity levels (Degens and Alway, 2006; Passey et al., 2016), we assessed the locomotor activity of the mice using an open field arena. Despite its prominent effect on muscle strength, IAV infection had no apparent effect on total distance travelled, irrespective of CS exposure (**Figure 4E**), hence physical inactivity is unlikely to contribute to the observed muscle weakness. These findings suggest that viral exacerbation primarily impacts muscle strength rather than mass, and this is not compounded by changes in locomotor activity.

### IAV Infection Evoked Oxidative Stress but did not Potentiate CS-Induced Disruption in Myogenic Signaling

Previous studies from our laboratory (Chan et al., 2021) and others (Barreiro et al., 2010; Fermoselle et al., 2012) have demonstrated the involvement of oxidative stress in CS-induced muscle dysfunction, however, its role in IAV infection remains unclear. An oxyblot assay on the TA muscle detected a 60% increase in protein carbonylation following IAV infection in Sham mice, and this was not further elevated when combined



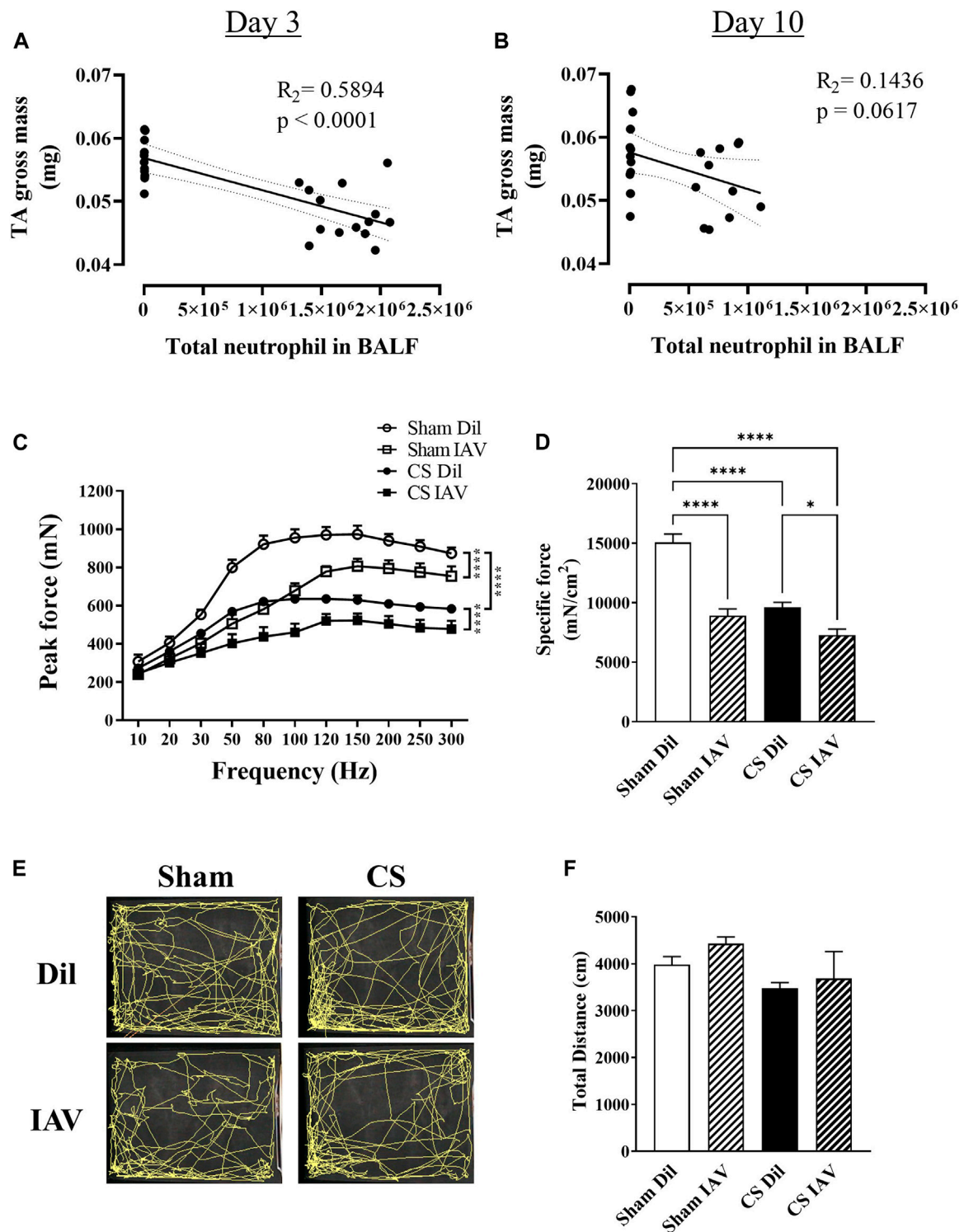


**FIGURE 4** | Effect of CS exposure and influenza A virus (IAV) infection on tibialis anterior (TA) muscle function. Correlational analyses of TA gross weight and total neutrophil counts in the BALF at **(A)** day 3 and **(B)** day 10 post IAV infection in CS-exposed and Sham mice. **(C)** Maximum contractile force and **(D)** specific force at 120 Hz were determined at peak of airway inflammation i.e., day 3. Prior to muscle functional analyses, recordings were made of locomotor activity over an 8-min period and **(E)** trace maps were generated and analyzed for total distance travelled (cm). Data shown as mean  $\pm$  SEM ( $n = 6$  per group for correlational and TA contractile function analyses, and  $n = 10$  per group for locomotor activity assessment). \* $p < 0.05$ , \*\*\*\* $p < 0.0001$ .

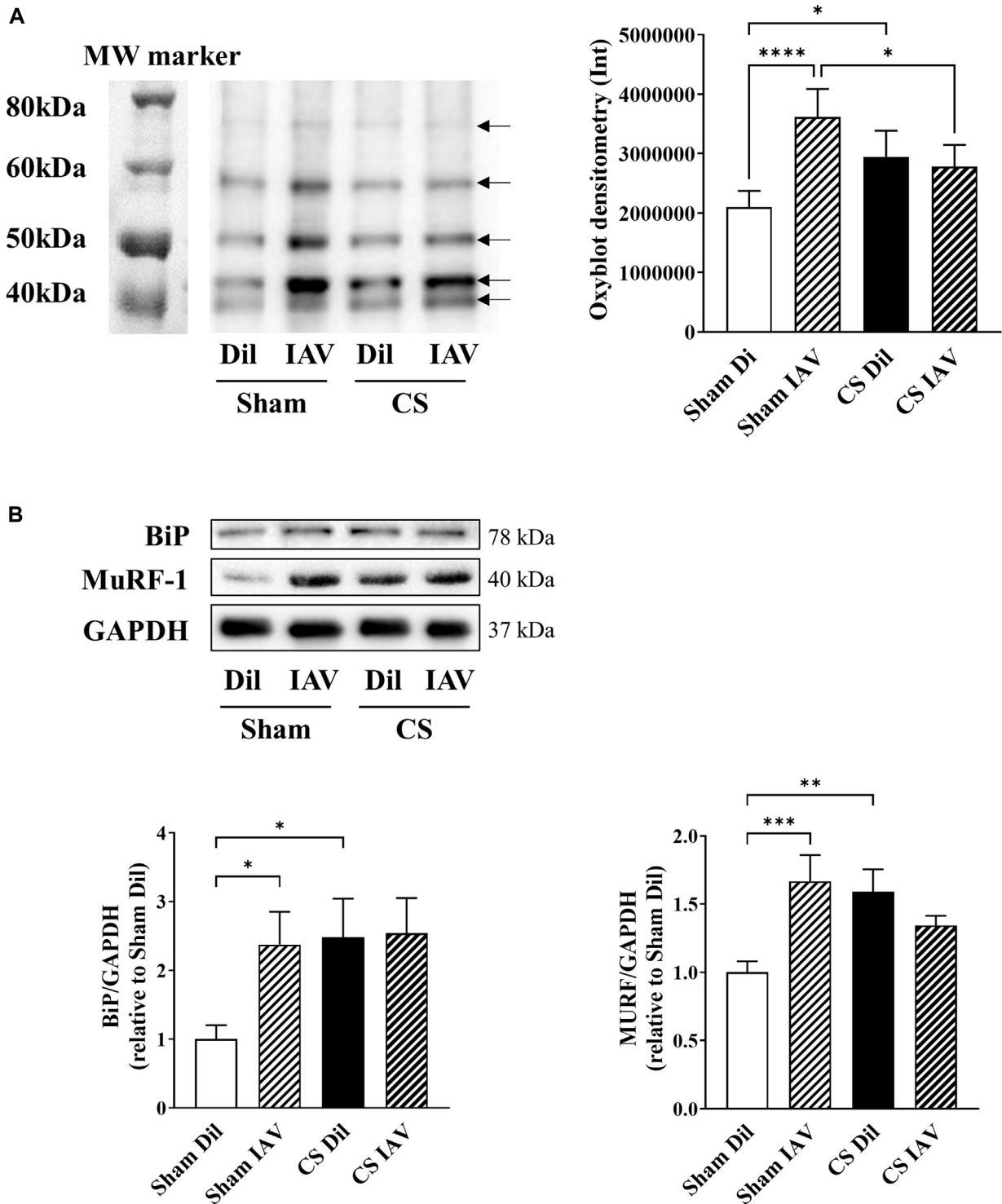
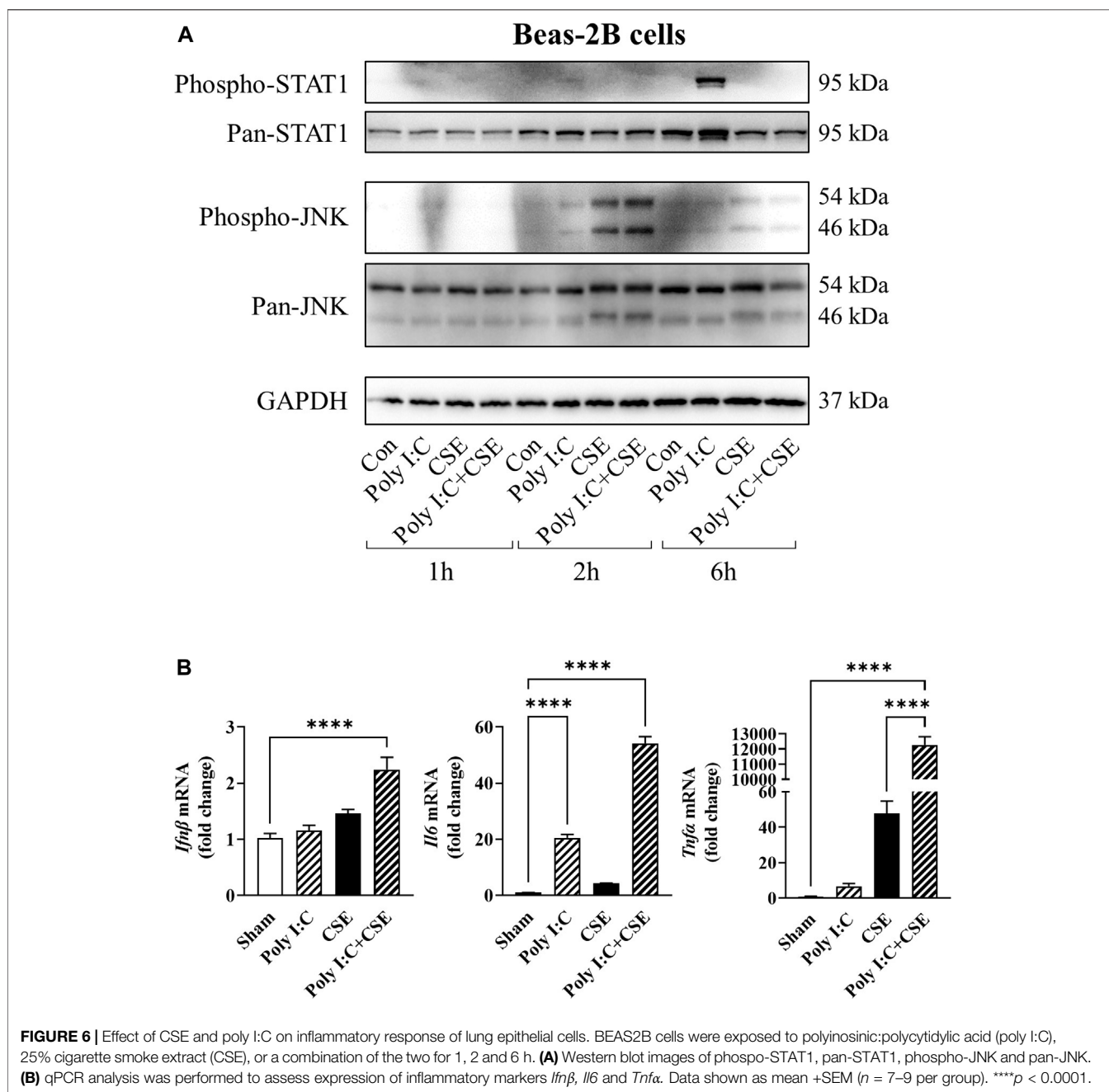


**FIGURE 5 |** Effect of CS exposure and influenza A virus (IAV) infection on oxidative stress and myogenic signaling in tibialis anterior (TA) of mice. Total protein carbonylation was measured using **(A)** Oxyblot staining and subsequent densitometry analysis on muscle homogenates of CS-exposed and Sham mice infected with IAV. Bands indicated by black arrows in densitometry were measured and added up for analysis. **(B)** Western blot images and quantitative densitometry analysis of BiP and MURF. Data shown as mean +SEM ( $n = 8$  per group). \* $p < 0.05$ , \*\* $p < 0.01$ , \*\*\* $p < 0.001$ , \*\*\*\* $p < 0.0001$ .

**TABLE 1** | Summary of gene expression data from the TA muscle (mean  $\pm$  SEM).

Gene name	Sham Dil	Sham IAV	CS Dil	CS IAV
<i>Cybb</i>	1.02 $\pm$ 0.05	15.39 $\pm$ 1.71 <sup>†††</sup>	1.08 $\pm$ 0.06	2.46 $\pm$ 0.24
<i>Gpx-1</i>	1.11 $\pm$ 0.12	2.92 $\pm$ 0.31 <sup>†††</sup>	1.90 $\pm$ 0.43	1.03 $\pm$ 0.11 <sup>***</sup>
<i>Myog</i>	1.15 $\pm$ 0.19	0.41 $\pm$ 0.07 <sup>†††</sup>	0.73 $\pm$ 0.04 <sup>*</sup>	0.33 $\pm$ 0.07 <sup>†</sup> <sup>§</sup>
<i>Mstn</i>	1.08 $\pm$ 0.10	10.69 $\pm$ 1.57 <sup>†††</sup>	17.15 $\pm$ 1.37 <sup>***</sup>	5.73 $\pm$ 0.93 <sup>*</sup> <sup>†††</sup> <sup>§§</sup>
<i>Myh7</i>	1.07 $\pm$ 0.11	0.65 $\pm$ 0.076 <sup>††</sup>	0.18 $\pm$ 0.02 <sup>***</sup>	0.40 $\pm$ 0.08 <sup>*</sup> <sup>§§§</sup>
<i>Tpm3</i>	1.11 $\pm$ 0.10	2.13 $\pm$ 0.34 <sup>†</sup>	2.15 $\pm$ 0.17 <sup>*</sup>	2.27 $\pm$ 0.28 <sup>§</sup>

\*  $p < 0.05$ , \*\*\*  $p < 0.001$  vs. the respective Sham; <sup>†</sup>  $p < 0.05$ , <sup>††</sup>  $p < 0.01$ , <sup>†††</sup>  $p < 0.001$  vs. the respective diluent-treated Sham/CS; <sup>§</sup>  $p < 0.05$ , <sup>§§</sup>  $p < 0.01$ , <sup>§§§</sup>  $p < 0.001$  vs. Sham Dil.



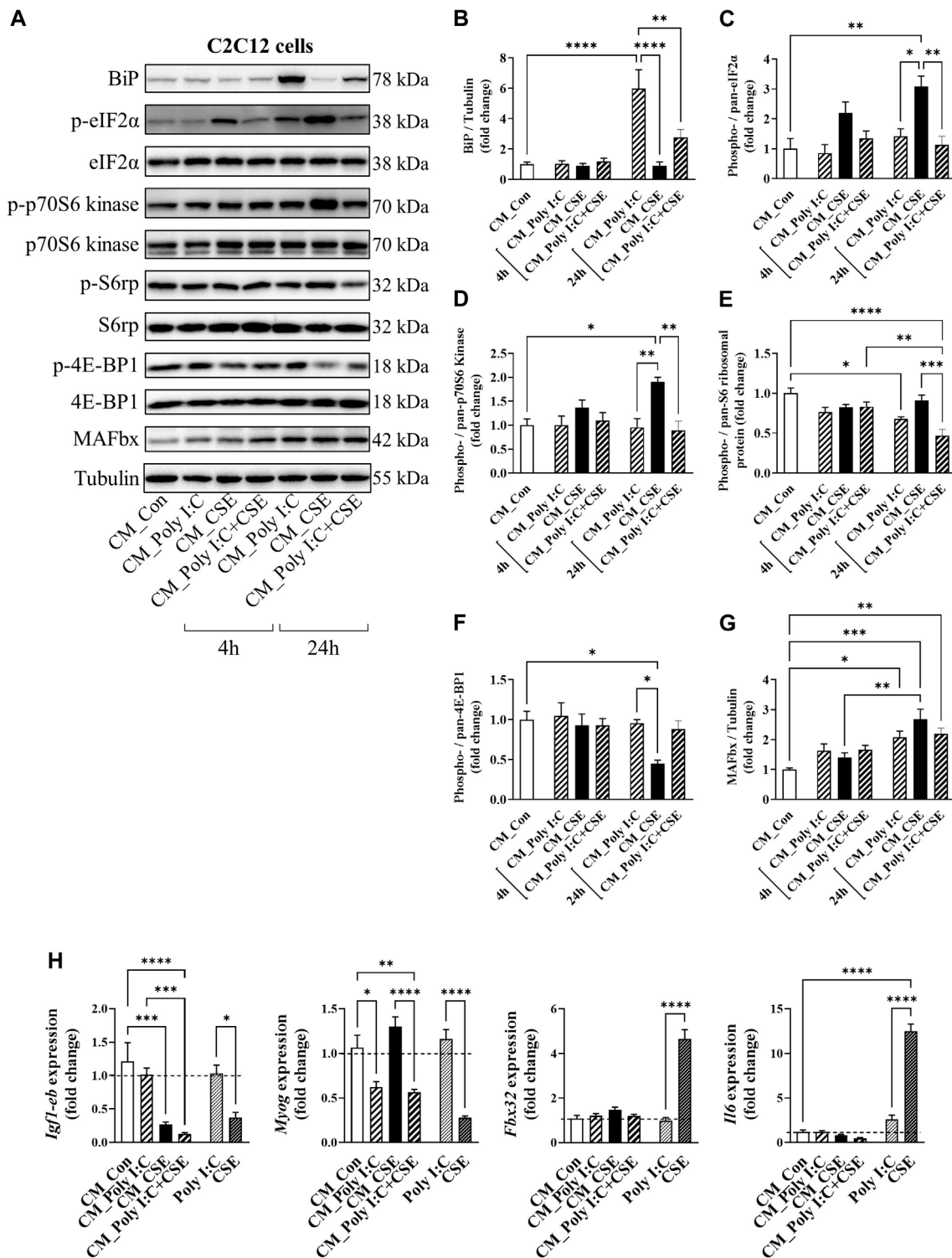


**FIGURE 7 |** Effect of cigarette smoke extract (CSE) and poly I:C conditioned media (CM) on proteostatic signaling of C2C12 myotubes. CM derived from BEAS2B cells exposed for 6 h to polyI:C, 25% CSE or a combination of the two was transferred onto differentiated C2C12 myotubes. **(A)** Western blot images and densitometry analysis of **(B)** BiP, **(C)** phospho (ser51)-/pan-eIF2α, **(D)** phospho (Thr389)-/pan-p70S6 kinase, **(E)** phospho (Ser235/236)-/pan- S6 ribosomal protein, **(F)** phospho (Thr37/46)-/pan- 4E-BP1, and **(G)** MAFbx. **(H)** qPCR analysis was performed to assess expression of *Igf1-cb*, *Myog*, *Fbx32* and *Il6*. Data shown as mean +SEM (n = 7–9 per group). \*p < 0.05, \*\*p < 0.01, \*\*\*p < 0.001, \*\*\*\*p < 0.0001.

with CS exposure (**Figure 5A**). At the molecular level, IAV infection elicited a 15-fold increase in *Cybb* [NADPH oxidase 2 (Nox2)] and a 3-fold increase in glutathione peroxidase 1 (*Gpx-1*) mRNA expression. However, this response appeared to be completely blunted when IAV infection was combined with CS exposure (**Table 1**). IAV infection also subdued myogenic signaling, characterized by a downregulation in mRNA expression of myogenin (*Myog*; 60% reduction), a positive regulator of myogenesis, and concomitant upregulation of myostatin (*Mstn*; 10-fold), which inhibits myogenesis, irrespective of CS exposure (**Table 1**). In line with the induction of oxidative stress and blunted myogenic signaling, the protein abundance of binding immunoglobulin protein (BiP) and muscle RING-finger protein-1 (MuRF-1) were markedly elevated by IAV infection, irrespective of CS exposure (**Figure 5B**). BiP is a cellular redox sensor and a master regulator of protein folding (Wang et al., 2014), while MuRF-1 is a downstream effector of myostatin that promotes ubiquitin-mediated protein degradation in skeletal muscle (Desgeorges et al., 2017). These findings imply that IAV infection does not further exacerbate the oxidative burden in the muscle or increase the disruption to myogenic signaling incurred by CS exposure.

### Exposure of Bronchial Epithelial Cells to TLR3 Activating Viral Mimetics Elicits STAT1 Activation and Accentuated the Expression of Pro-Inflammatory Cytokines

To ascertain the contributory role of airway inflammation in the disruption of myogenic signaling, we treated bronchial epithelial cells (BEAS-2B) with poly I:C, a well-established viral mimetic used to exacerbate inflammation in lung injury models (Vella et al., 2020), in the presence or absence of CSE, to recapitulate a viral exacerbation. Poly I:C stimulated the phosphorylation of signal transducer and activator of transcription 1 (STAT1; **Figure 6A**) and resulted in a 20-fold increase in the expression of interleukin-6 (*Il-6*; **Figure 6B**). In contrast, CSE elicited rapid phosphorylation of c-Jun N-terminal kinase (JNK) which was accompanied by an increased expression of tumor necrosis factor  $\alpha$  (*Tnfa*; **Figures 6A,B**). Although cell viability was seemingly unaltered (**Supplementary Figure S1A**), co-exposure to poly I:C and CSE resulted in a marked increase in interferon  $\beta$  (*Ifn $\beta$* ; 2.4-fold), *Il-6* (54-fold) and *Tnfa* (~12,000-fold) mRNA expression, suggesting an amplified toll-like receptor (TLR)-3-driven inflammatory response in these bronchial epithelial cells.

### Amplified Lung Cell Inflammation did not Potentiate Myogenic Disruption Driven by CSE

To determine whether the TLR3-driven inflammatory response of the lung cells may potentiate myogenic disruption by CSE, we transferred the culture medium of the BEAS-2B cells (i.e., CM) onto C2C12 myotubes for a time-course experiment, as outlined in **Figure 7**. Myotubes

treated acutely (4-h exposure), with CM from poly I:C-treated cells displayed no observable changes in key signal transducers of protein folding [BiP, eukaryotic initiation factor 2 $\alpha$  (eIF2 $\alpha$ )], protein synthesis [p70 S6 Kinase, S6 ribosomal protein, eukaryotic translation initiation factor 4E-binding protein 1 (4E-BP1)] or in muscle-specific F-box (MAFbx); a negative regulator of muscle mass (Passey et al., 2016). Despite not having an apparent effect on the structural integrity of the myotubes (**Supplementary Figure S1B**), 24-h exposure to the poly I:C CM resulted in a marked increase in BiP and eIF2 $\alpha$  phosphorylation (**Figures 7A–C**), suppression of S6 ribosomal protein phosphorylation (**Figures 7A,E**), and elevation of MAFbx abundance (**Figures 7A,G**), suggesting a shift in myogenic balance. CM from CSE-exposed cells had distinct impacts on the myogenic signaling, characterized by an even greater phosphorylation of eIF2 $\alpha$  without an increase in BiP protein expression (**Figure 7B**), increased p70 S6 Kinase phosphorylation (**Figure 7D**), diminished 4E-BP1 phosphorylation (**Figure 7F**) and a concomitant increase in MAFbx protein expression (**Figure 7G**). CM from the poly I:C + CSE-exposed lung cells increased BiP and MAFbx abundance, like the poly I:C alone experiments, and furthermore, significantly suppressed the phosphorylation of S6 ribosomal protein.

We next performed qPCR on the CM-exposed myotubes for markers of myogenesis and inflammation. Unlike CSE, direct stimulation of C2C12 myotubes with poly I:C had no significant impact on myogenic genes and *Il6* expression (**Figure 7H**). Similar to what was seen in our *in vivo* IAV infection model (**Table 1**), poly I:C CM caused a ~50% reduction in *Myog* mRNA expression, without any significant changes observed in the gene expression of either *Fbx32*, which encodes for the MAFbx protein, or *Il6* (**Figure 7H**). Importantly, CM from poly I:C + CSE did not further increase these changes, suggesting the TLR3-driven inflammatory response of the lung cells is unlikely to have an additive effect on myogenic disruption driven by CSE.

## DISCUSSION

Skeletal muscle dysfunction is a common comorbidity amongst people with COPD and is often worsened during/following an acute exacerbation (Güerri et al., 2010; Greening et al., 2015; Perrot et al., 2020). The present study aimed to examine how acute exacerbation by IAV infection promotes muscle dysfunction, focusing on the contributory role of airway inflammation in this process. Our results demonstrated that IAV infection amplified CS-induced airway inflammation and limb muscle weakness without further impacting muscle mass. Although, IAV infection alone evoked oxidative stress in the TA, viral exacerbation did not further elevate oxidative stress levels or disruptions to myogenic signaling induced by CS exposure, suggesting airway inflammation is independent to the observed muscle loss. We next used an *in vitro* CM approach to further investigate this relationship. Despite an accentuated inflammatory response in the lung cells due to the activation of TLR3/STAT1, the combination of viral mimetics and CSE did not

exert additive effects on myogenic signaling. Hence, airway inflammation is unlikely to be the sole driving force for the further deteriorated muscle dysfunction observed during AECOPD.

In COPD, neutrophilic recruitment into the lungs is directly correlated with disease severity and worsened respiratory symptoms including increased sputum production and breathlessness (Meijer et al., 2013). During infectious AECOPD, airway neutrophilia becomes even more prominent compared to stable COPD (Papi et al., 2006; Oostwoud et al., 2016), with recruited neutrophils being more activated, potentially driving further inflammation, and thereby increasing tissue damage and airway dysfunction (Johansson and Kirsebom, 2021). In line with this, our data showed that upon viral exacerbation, neutrophilia and total cellularity in the BALF were significantly increased at both day 3 and 10 timepoints, confirming the presence of an exuberant airway inflammation in our *in vivo* model that is characteristic of human AECOPD (Bozinovski et al., 2012; Wang et al., 2019).

Amplified airway inflammation evoked by infectious exacerbations have been shown to further the limb muscle loss seen in AECOPD (Perera et al., 2007; Rubinsztajn et al., 2014). In accordance with this, we detected a significant negative correlation between the loss of TA muscle mass and BALF neutrophilia on day 3, but not day 10 post-infection. This finding suggests there is a link between the peak of airway inflammation and the manifestation of muscle loss during AECOPD. However, the gross weight of the leg muscles was not further reduced following viral exacerbation, and this observation was substantiated by the lack of change in mean myofiber area, and the absence of further disruptions to myogenic signaling. This suggests a single episode of viral exacerbation may not necessarily add to the COPD-related muscle loss, despite the presence of an accentuated airway inflammation. Guerri *et al.* (Guerri et al., 2010) observed a greater loss of limb muscle CSA in individuals who suffered from four or more episodes of AECOPD compared to individuals who only experienced a single exacerbation, highlighting the compounding effect of repeated exacerbation on limb muscle impairment.

Our *in vitro* experiments revealed that viral exacerbation CM did not incur further myogenic disruption or impact on cell viability. Of note, myotube loss and degradation of sarcomere structures were found following 48 h of exposure to CSE CM, which was not observed following exposure to Poly I:C CM. Direct exposure to poly I:C resulted in no myogenic disruption, suggesting the muscle cells are unresponsive to poly I:C even though TLR3 has been reported to be expressed in myotubes (Cho et al., 2017). Taken together, these data support the notion that TLR3/STAT1-driven airway inflammation does not potentiate COPD-related muscle loss.

Another main finding of the present study is that viral exacerbation drove a further impairment in contractile strength of the TA muscle of CS-exposed mice, despite no further reduction in muscle mass or mean myofiber CSA. This effect was persistent after adjusting for differences in muscle size, thus confirming the additive impact of viral exacerbation on muscle weakness. The TA is the strongest dorsiflexor muscle of

the foot and is critical to gait as dorsiflexion clears the foot off of the ground during the swing phase (Hardin and Devendra, 2022). Therefore, we assessed locomotor activity to ascertain whether this exacerbation-related muscle weakness impacted gait, which is believed to play a major role in the exercise limitation observed clinically in individuals with COPD (Maltais et al., 2014). Surprisingly, neither CS exposure nor viral exacerbation had a significant impact on locomotor activity, despite a >50% reduction in the force generating capacity of the TA.

This brings about several important observations: i) impairment in contractile capacity and muscle mass loss may precede the manifestation of changes in locomotor activity; ii) contractile function may be more sensitive to exacerbation-related impairments than muscle mass; iii) limb muscle dysfunction can occur independent of physical inactivity, which is conceptually important as physical inactivity is a major contributor to muscle dysfunction, and infectious exacerbations are known to make patients become even less active (Pitta et al., 2005). If exacerbation-driven airway inflammation itself does not directly worsen limb muscle dysfunction, the question remains as to what causes the further muscle impairments observed during AECOPD. The cause of muscle dysfunction in this context is likely to be multifactorial, involving both conventional and unconventional factors such as unintended weight loss, length of hospitalization, glucocorticoids use and epigenetics (Passey et al., 2016). However, one should also be mindful of the locomotion/postural differences between rodent (quadrupedal) versus human (bipedal), which implies that the locomotor impact of limb muscle weakness may be more significant in human than in mice.

Despite the multifactorial nature, muscle impairments in stable COPD and AECOPD can be effectively targeted with nutritional interventions and exercise therapy (Passey et al., 2016). However, both nutritional interventions and exercise therapy may not always be feasible in patients with severe respiratory or limb muscle impairments, thus making pharmacologic approaches an important modality of treatment (van Bakel et al., 2021). The use of anabolic hormones, such as testosterone has been demonstrated to acutely improve muscle loss and dysfunction in patients with COPD (Casaburi et al., 2004), presumably *via* the IGF-1 pathway (Passey et al., 2016). It should be noted that hormone replacement therapies are often associated with adverse side-effects and the long-term benefits of anabolic hormone supplement remain to be established. The observation that IGF-1 is only positively related to muscle strength when circulating levels of IL-6 is low (Barbieri et al., 2003) raises an important notion that the effectiveness of anabolic hormone therapy may be negative influenced by systemic inflammation, which is a hallmark feature of advanced COPD (Hillas et al., 2016). Inhibition of protein degradation in muscle has been explored as a potential therapy, though inhibition of autophagy (Masiero et al., 2009) or ubiquitin-proteasome system (Kitajima et al., 2014) have paradoxically resulted in muscle loss. The strong involvement of oxidative stress in the pathophysiology of both lung and limb muscle dysfunction has prompted the importance of targeting oxidative stress.

Indeed, recent data from our laboratory demonstrated that apocynin, a free radical scavenger and a Nox2 inhibitor, attenuated airway inflammation and muscle impairments by CS exposure (Chan et al., 2021), suggesting the effectiveness and feasibility of targeting oxidative stress by pharmacological means to treat lung and systemic manifestations of COPD.

In summary, the present study demonstrated that viral exacerbation may deteriorate muscle weakness without additive effects on muscle loss. This may be explained in part by the minimal impacts of TLR3-driven airway inflammation on muscle cells. Our data also showed that muscle cells are relatively unresponsive to direct TLR3 stimulation, thus ruling out the possibility of endogenous TLR3 signaling in driving myogenic disruption. The findings of the present study prompt further research questions, particularly surrounding 1) the differences in IAV strains, and 2) the compounding effect of repeated viral exacerbations. It is known that different strains of IAV have different pathogenicity, and the strain used in the present study (Mem71) is considered to be of intermediate pathogenicity compared to other strains (Ong et al., 2017). Of note, severe IAV pneumonia caused by the A/WSN/33 strain has been demonstrated to directly promote muscle loss in mice, in an IL-6 dependent manner (Radigan et al., 2019). Meanwhile repeated episodes of exacerbations are known to aggravate not only respiratory symptoms, but also systemic comorbidities such as muscle dysfunction (Anzueto, 2010). Of interest, even a single episode of IAV-induced exacerbation by the Mem71 strain has been shown to provoke airway hypersensitivity to future allergen challenge, despite the initial IAV-induced bronchoalveolar inflammation had long subsided (Looi et al., 2021), suggesting an increased risk for future exacerbations. Therefore, future studies should examine the strain discrepancies of IAV (including impacts of viral loading and their respective impacts to disease outcomes) and the compounding impacts of repeated exacerbations to provide a more complete picture of the impacts of AECOPD on limb muscle dysfunction.

## REFERENCES

- Amado, C. A., García-Unzueta, M. T., Lavin, B. A., Guerra, A. R., Agüero, J., Ramos, L., et al. (2019). The Ratio Serum Creatinine/Serum Cystatin C (A Surrogate Marker of Muscle Mass) as a Predictor of Hospitalization in Chronic Obstructive Pulmonary Disease Outpatients. *Respiration* 97 (4), 302–309. doi:10.1159/000494296
- Anzueto, A. (2010). Impact of Exacerbations on COPD. *Eur. Respir. Rev.* 19 (116), 113–118. doi:10.1183/09059180.00002610
- Barbieri, M., Ferrucci, L., Ragno, E., Corsi, A., Bandinelli, S., Bonafè, M., et al. (2003). Chronic Inflammation and the Effect of IGF-I on Muscle Strength and Power in Older Persons. *Am. J. Physiol. Endocrinol. Metab.* 284, E481–E487. doi:10.1152/ajpendo.00319.2002
- Barnes, P. J., and Celli, B. R. (2009). Systemic Manifestations and Comorbidities of COPD. *Eur. Respir. J.* 33 (5), 1165–1185. doi:10.1183/09031936.00128008
- Barnes, P. J. (2017). Cellular and Molecular Mechanisms of Asthma and COPD. *Clin. Sci. (Lond)* 131 (13), 1541–1558. doi:10.1042/CS20160487

## DATA AVAILABILITY STATEMENT

The original contributions presented in the study are included in the article/**Supplementary Material**, further inquiries can be directed to the corresponding author.

## ETHICS STATEMENT

All experimental procedures and protocols were conducted in accordance with the Australian Code of Practice for the Care and Use of Animals for Scientific Purposes and approved by the RMIT University Animal Ethics Committee (AEC 1533).

## AUTHOR CONTRIBUTIONS

Concept and design: RV and SMHC; acquisition of data: KM, SMHC, KB, AD, SND, and HJS; data analysis and interpretation: KM, SMHC, RV, SND, SS, and SB; technical assistance: KB, AD, and HJS; drafting, editing, and/or critical revision of the manuscript for intellectual content: all authors; RV also provided all resources for the work and is the senior investigator, ensuring accuracy and integrity.

## FUNDING

The authors would like to thank the National Health and Medical Research Council of Australia (Project Grant Numbers APP1084627 and APP1138915) for funding this work.

## SUPPLEMENTARY MATERIAL

The Supplementary Material for this article can be found online at: <https://www.frontiersin.org/articles/10.3389/fphar.2022.859146/full#supplementary-material>

- Barnes, P. J. (2018). Targeting Cytokines to Treat Asthma and Chronic Obstructive Pulmonary Disease. *Nat. Rev. Immunol.* 18 (7), 454–466. doi:10.1038/s41577-018-0006-6
- Barreiro, E., Peinado, V. I., Galdiz, J. B., Ferrer, E., Marin-Corral, J., Sánchez, F., et al. (2010). Cigarette Smoke-Induced Oxidative Stress: A Role in Chronic Obstructive Pulmonary Disease Skeletal Muscle Dysfunction. *Am. J. Respir. Crit. Care Med.* 182 (4), 477–488. doi:10.1164/rccm.200908-1220OC
- Bernard, S., LeBlanc, P., Whittom, F., Carrier, G., Jobin, J., Belleau, R., et al. (1998). Peripheral Muscle Weakness in Patients with Chronic Obstructive Pulmonary Disease. *Am. J. Respir. Crit. Care Med.* 158 (2), 629–634. doi:10.1164/ajrccm.158.2.9711023
- Bernardo, I., Bozinovski, S., and Vlahos, R. (2015). Targeting Oxidant-dependent Mechanisms for the Treatment of COPD and its Comorbidities. *Pharmacol. Ther.* 155, 60–79. doi:10.1016/j.pharmthera.2015.08.005
- Bozinovski, S., Uddin, M., Vlahos, R., Thompson, M., McQualter, J. L., Merritt, A. S., et al. (2012). Serum Amyloid A Opposes Lipoxin A<sub>4</sub> to Mediate Glucocorticoid Refractory Lung Inflammation in Chronic Obstructive Pulmonary Disease. *Proc. Natl. Acad. Sci. U S A.* 109 (3), 935–940. doi:10.1073/pnas.1109382109

- Casaburi, R., Bhasin, S., Cosentino, L., Porszasz, J., Somfay, A., Lewis, M. I., et al. (2004). Effects of Testosterone and Resistance Training in Men with Chronic Obstructive Pulmonary Disease. *Am. J. Respir. Crit. Care Med.* 170 (8), 870–878. doi:10.1164/rccm.200305-617OC
- Chan, S. M. H., Bernardo, I., Mastronardo, C., Mou, K., De Luca, S. N., Seow, H. J., et al. (2021). Apocynin Prevents Cigarette Smoking-Induced Loss of Skeletal Muscle Mass and Function in Mice by Preserving Proteostatic Signalling. *Br. J. Pharmacol.* 178 (15), 3049–3066. doi:10.1111/bph.15482
- Chan, S. M. H., Cerni, C., Passey, S., Seow, H. J., Bernardo, I., van der Poel, C., et al. (2020). Cigarette Smoking Exacerbates Skeletal Muscle Injury without Compromising its Regenerative Capacity. *Am. J. Respir. Cell Mol Biol* 62 (2), 217–230. doi:10.1165/rcmb.2019-0106OC
- Cho, K. A., Park, M., Kim, Y. H., Woo, S. Y., and Ryu, K. H. (2017). Conditioned media from Human palatine Tonsil Mesenchymal Stem Cells Regulates the Interaction between Myotubes and Fibroblasts by IL-1Ra Activity. *J. Cell Mol Med* 21 (1), 130–141. doi:10.1111/jcmm.12947
- Decramer, M., and Janssens, W. (2013). Chronic Obstructive Pulmonary Disease and Comorbidities. *Lancet Respir. Med.* 1 (1), 73–83. doi:10.1016/S2213-2600(12)70060-7
- Degens, H., and Alway, S. E. (2006). Control of Muscle Size during Disuse, Disease, and Aging. *Int. J. Sports Med.* 27 (2), 94–99. doi:10.1055/s-2005-837571
- Desgeorges, M. M., Devillard, X., Toutain, J., Castells, J., Divoux, D., Arnold, D. F., et al. (2017). Pharmacological Inhibition of Myostatin Improves Skeletal Muscle Mass and Function in a Mouse Model of Stroke. *Sci. Rep.* 7 (1), 14000. doi:10.1038/s41598-017-13912-0
- Fermoselle, C., Rabinovich, R., Ausin, P., Puig-Vilanova, E., Coronell, C., Sanchez, F., et al. (2012). Does Oxidative Stress Modulate Limb Muscle Atrophy in Severe COPD Patients? *Eur. Respir. J.* 40 (4), 851–862. doi:10.1183/09031936.00137211
- Files, D. C., D'Alessio, F. R., Johnston, L. F., Kesari, P., Aggarwal, N. R., Garibaldi, B. T., et al. (2012). A Critical Role for Muscle Ring finger-1 in Acute Lung Injury-Associated Skeletal Muscle Wasting. *Am. J. Respir. Crit. Care Med.* 185 (8), 825–834. doi:10.1164/rccm.201106-1150OC
- Girón, R., Matesanz, C., García-Río, F., de Santiago, E., Mancha, A., Rodríguez-Salvanes, F., et al. (2009). Nutritional State during COPD Exacerbation: Clinical and Prognostic Implications. *Ann. Nutr. Metab.* 54 (1), 52–58. doi:10.1159/000205960
- Gompertz, S., O'Brien, C., Bayley, D. L., Hill, S. L., and Stockley, R. A. (2001). Changes in Bronchial Inflammation during Acute Exacerbations of Chronic Bronchitis. *Eur. Respir. J.* 17 (6), 1112–1119. doi:10.1183/09031936.01.99114901
- Gosker, H. R., Langen, R. C., and Simons, S. O. (2021). Role of Acute Exacerbations in Skeletal Muscle Impairment in COPD. *Expert Rev. Respir. Med.* 15 (1), 103–115. doi:10.1080/17476348.2021.1843429
- Gosker, H. R., Zeegers, M. P., Wouters, E. F., and Schols, A. M. (2007). Muscle Fibre Type Shifting in the Vastus Lateralis of Patients with COPD Is Associated with Disease Severity: a Systematic Review and Meta-Analysis. *Thorax* 62 (11), 944–949. doi:10.1136/thx.2007.078980
- Gosselink, R., Troosters, T., and Decramer, M. (1996). Peripheral Muscle Weakness Contributes to Exercise Limitation in COPD. *Am. J. Respir. Crit. Care Med.* 153 (3), 976–980. doi:10.1164/ajrccm.153.3.8630582
- Greening, N. J., Harvey-Dunstan, T. C., Chaplin, E. J., Vincent, E. E., Morgan, M. D., Singh, S. J., et al. (2015). Bedside Assessment of Quadriceps Muscle by Ultrasound after Admission for Acute Exacerbations of Chronic Respiratory Disease. *Am. J. Respir. Crit. Care Med.* 192 (7), 810–816. doi:10.1164/rccm.201503-0535OC
- Gualano, R. C., Hansen, M. J., Vlahos, R., Jones, J. E., Park-Jones, R. A., Deliyannis, G., et al. (2008). Cigarette Smoke Worsens Lung Inflammation and Impairs Resolution of Influenza Infection in Mice. *Respir. Res.* 9, 53. doi:10.1186/1465-9921-9-53
- Guerri, R., Gayete, A., Balcells, E., Ramirez-Sarmiento, A., Vollmer, I., Garcia-Aymerich, J., et al. (2010). Mass of Intercostal Muscles Associates with Risk of Multiple Exacerbations in COPD. *Respir. Med.* 104 (3), 378–388. doi:10.1016/j.rmed.2009.10.015
- Hardin, J. M., and Devendra, S. (2022). “Anatomy, Bony Pelvis and Lower Limb, Calf Common Peroneal (Fibular) Nerve,” in *StatPearls* (Treasure Island, FL: StatPearls Publishing LLC). StatPearls Publishing Copyright © 2021.
- Hillas, G., Perlikos, F., Toumpanakis, D., Litsiou, E., Nikolakopoulou, S., Sagris, K., et al. (2016). Controlled Mechanical Ventilation Attenuates the Systemic Inflammation of Severe Chronic Obstructive Pulmonary Disease Exacerbations. *Am. J. Respir. Crit. Care Med.* 193 (6), 696–698. doi:10.1164/rccm.201508-1700LE
- Hoenderdos, K., and Condliffe, A. (2013). The Neutrophil in Chronic Obstructive Pulmonary Disease. *Am. J. Respir. Cell Mol Biol* 48 (5), 531–539. doi:10.1165/rcmb.2012-0492TR
- Johansson, C., and Kirsebom, F. C. M. (2021). Neutrophils in Respiratory Viral Infections. *Mucosal Immunol.* 14 (4), 815–827. doi:10.1038/s41385-021-00397-4
- Kitajima, Y., Tashiro, Y., Suzuki, N., Warita, H., Kato, M., Tateyama, M., et al. (2014). Proteasome Dysfunction Induces Muscle Growth Defects and Protein Aggregation. *J. Cell Sci* 127 (Pt 24), 5204–5217. doi:10.1242/jcs.150961
- Looi, K., Larcombe, A. N., Perks, K. L., Berry, L. J., Zosky, G. R., Rigby, P., et al. (2021). Previous Influenza Infection Exacerbates Allergen Specific Response and Impairs Airway Barrier Integrity in Pre-sensitized Mice. *Int. J. Mol. Sci.* 22, 22. doi:10.3390/ijms22168790
- Mackay, A. J., and Hurst, J. R. (2013). COPD Exacerbations: Causes, Prevention, and Treatment. *Immunol. Allergy Clin. North. Am.* 33 (1), 95–115. doi:10.1016/j.jiac.2012.10.006
- Maltais, F., Decramer, M., Casaburi, R., Barreiro, E., Burelle, Y., Debigaré, R., et al. (2014). An Official American Thoracic Society/European Respiratory Society Statement: Update on Limb Muscle Dysfunction in Chronic Obstructive Pulmonary Disease. *Am. J. Respir. Crit. Care Med.* 189, e15–62. doi:10.1164/rccm.201402-0373ST
- Marquis, K., Debigaré, R., Lacasse, Y., LeBlanc, P., Jobin, J., Carrier, G., et al. (2002). Midhigh Muscle Cross-Sectional Area Is a Better Predictor of Mortality Than Body Mass index in Patients with Chronic Obstructive Pulmonary Disease. *Am. J. Respir. Crit. Care Med.* 166 (6), 809–813. doi:10.1164/rccm.2107031
- Masiero, E., Agatea, L., Mammucari, C., Blaauw, B., Loro, E., Komatsu, M., et al. (2009). Autophagy Is Required to Maintain Muscle Mass. *Cell Metab* 10 (6), 507–515. doi:10.1016/j.cmet.2009.10.008
- Mathioudakis, A. G., Janssens, W., Sivapalan, P., Singanayagam, A., Dransfield, M. T., Jensen, J. S., et al. (2020). Acute Exacerbations of Chronic Obstructive Pulmonary Disease: in Search of Diagnostic Biomarkers and Treatable Traits. *Thorax* 75 (6), 520–527. doi:10.1136/thoraxjnl-2019-214484
- Meijer, M., Rijkers, G. T., and van Overveld, F. J. (2013). Neutrophils and Emerging Targets for Treatment in Chronic Obstructive Pulmonary Disease. *Expert Rev. Clin. Immunol.* 9 (11), 1055–1068. doi:10.1586/1744666X.2013.851347
- Mohammadipoor, A., Antebi, B., Batchinsky, A. I., and Cancio, L. C. (2018). Therapeutic Potential of Products Derived from Mesenchymal Stem/stromal Cells in Pulmonary Disease. *Respir. Res.* 19 (1), 218. doi:10.1186/s12931-018-0921-x
- Ong, J. D., Mansell, A., and Tate, M. D. (2017). Hero Turned Villain: NLRP3 Inflammasome-Induced Inflammation during Influenza A Virus Infection. *J. Leukoc. Biol.* 101 (4), 863–874. doi:10.1189/jlb.4MR0616-288R
- Oostwoud, L. C., Gunasinghe, P., Seow, H. J., Ye, J. M., Selemidis, S., Bozinovski, S., et al. (2016). Apocynin and Ebselen Reduce Influenza A Virus-Induced Lung Inflammation in Cigarette Smoke-Exposed Mice. *Sci. Rep.* 6, 20983. doi:10.1038/srep20983
- Pan, L., Wang, M., Xie, X., Du, C., and Guo, Y. (2014). Effects of Anabolic Steroids on Chronic Obstructive Pulmonary Disease: a Meta-Analysis of Randomised Controlled Trials. *PLoS One* 9, e84855. doi:10.1371/journal.pone.0084855
- Papi, A., Bellettato, C. M., Braccioni, F., Romagnoli, M., Casolari, P., Caramori, G., et al. (2006). Infections and Airway Inflammation in Chronic Obstructive Pulmonary Disease Severe Exacerbations. *Am. J. Respir. Crit. Care Med.* 173 (10), 1114–1121. doi:10.1164/rccm.200506-859OC
- Passey, S. L., Hansen, M. J., Bozinovski, S., McDonald, C. F., Holland, A. E., and Vlahos, R. (2016). Emerging Therapies for the Treatment of Skeletal Muscle Wasting in Chronic Obstructive Pulmonary Disease. *Pharmacol. Ther.* 166, 56–70. doi:10.1016/j.pharmthera.2016.06.013
- Perera, W. R., Hurst, J. R., Wilkinson, T. M., Sapsford, R. J., Müllerova, H., Donaldson, G. C., et al. (2007). Inflammatory Changes, Recovery and Recurrence at COPD Exacerbation. *Eur. Respir. J.* 29 (3), 527–534. doi:10.1183/09031936.00092506



- Perrot, L., Greil, A., Boirie, Y., Farigon, N., Mulliez, A., Costes, F., et al. (2020). Prevalence of Sarcopenia and Malnutrition during Acute Exacerbation of COPD and after 6 Months Recovery. *Eur. J. Clin. Nutr.* 74 (11), 1556–1564. doi:10.1038/s41430-020-0623-6
- Pitta, F., Troosters, T., Spruit, M. A., Decramer, M., and Gosselink, R. (2005). Activity Monitoring for Assessment of Physical Activities in Daily Life in Patients with Chronic Obstructive Pulmonary Disease. *Arch. Phys. Med. Rehabil.* 86 (10), 1979–1985. doi:10.1016/j.apmr.2005.04.016
- Radigan, K. A., Nicholson, T. T., Welch, L. C., Chi, M., Amarelle, L., Angulo, M., et al. (2019). Influenza A Virus Infection Induces Muscle Wasting via IL-6 Regulation of the E3 Ubiquitin Ligase Atrogin-1. *J. Immunol.* 202 (2), 484–493. doi:10.4049/jimmunol.1701433
- Reading, P. C., Morey, L. S., Crouch, E. C., and Anders, E. M. (1997). Collectin-mediated Antiviral Host Defense of the Lung: Evidence from Influenza Virus Infection of Mice. *J. Virol.* 71 (11), 8204–8212. doi:10.1128/JVI.71.11.8204-8212.1997
- Rubinsztajn, R., Przybyłowski, T., Maskey-Warzęchowska, M., Karwat, K., Papińska-Goryca, M., Nejman-Gryz, P., et al. (2014). Effect of Exacerbation Frequency on Body Composition and Serum Ghrelin and Adiponectin Concentrations in Patients with Chronic Obstructive Pulmonary Disease. *Pol. Arch. Med. Wewn* 124 (7-8), 403–409. doi:10.20452/pamw.2351
- Schols, A. M., Broekhuizen, R., Weling-Scheepers, C. A., and Wouters, E. F. (2005). Body Composition and Mortality in Chronic Obstructive Pulmonary Disease. *Am. J. Clin. Nutr.* 82 (1), 53–59. doi:10.1093/ajcn.82.1.53
- van Bakel, S. I., Gosker, H. R., Langen, R. C., and Schols, A. M. (2021). Towards Personalized Management of Sarcopenia in COPD. *Copd* 16, 25–40. doi:10.2147/copd.s280540
- Vanfleteren, L. E. G. W., Spruit, M. A., Wouters, E. F. M., and Franssen, F. M. E. (2016). Management of Chronic Obstructive Pulmonary Disease beyond the Lungs. *Lancet Respir. Med.* 4 (11), 911–924. doi:10.1016/S2213-2600(16)00097-7
- Vella, G., Lunding, L., Ritzmann, F., Honecker, A., Herr, C., Wegmann, M., et al. (2020). The IL-17 Receptor IL-17RE Mediates polyIC-Induced Exacerbation of Experimental Allergic Asthma. *Respir. Res.* 21 (1), 176. doi:10.1186/s12931-020-01434-9
- Vlahos, R., Bozinovski, S., Jones, J. E., Powell, J., Gras, J., Lilja, A., et al. (2006). Differential Protease, Innate Immunity, and NF-kappaB Induction Profiles during Lung Inflammation Induced by Subchronic Cigarette Smoke Exposure in Mice. *Am. J. Physiol. Lung Cell Mol Physiol* 290, L931–L945. doi:10.1152/ajplung.00201.2005
- Vlahos, R., and Bozinovski, S. (2014). Recent Advances in Pre-clinical Mouse Models of COPD. *Clin. Sci. (Lond)* 126 (4), 253–265. doi:10.1042/CS20130182
- Vogelmeier, C. F., Criner, G. J., Martinez, F. J., Anzueto, A., Barnes, P. J., Bourbeau, J., et al. (2017). Global Strategy for the Diagnosis, Management, and Prevention of Chronic Obstructive Lung Disease 2017 Report: GOLD Executive Summary. *J. Respir. Crit. Care Med.* 195 (5), 557–582. doi:10.1183/13993003.50214-2017
- Wang, H., Aloe, C., Wilson, N., and Bozinovski, S. (2019). G-CSFR Antagonism Reduces Neutrophilic Inflammation during Pneumococcal and Influenza Respiratory Infections without Compromising Clearance. *Sci. Rep.* 9 (1), 17732. doi:10.1038/s41598-019-54053-w
- Wang, J., Pareja, K. A., Kaiser, C. A., and Sevier, C. S. (2014). Redox Signaling via the Molecular Chaperone BiP Protects Cells against Endoplasmic Reticulum-Derived Oxidative Stress. *Elife* 3, e03496. doi:10.7554/eLife.03496
- Conflict of Interest:** The authors declare that the research was conducted in the absence of any commercial or financial relationships that could be construed as a potential conflict of interest.
- Publisher's Note:** All claims expressed in this article are solely those of the authors and do not necessarily represent those of their affiliated organizations or those of the publisher, the editors, and the reviewers. Any product that may be evaluated in this article, or claim that may be made by its manufacturer, is not guaranteed or endorsed by the publisher.
- Copyright © 2022 Mou, Chan, Brassington, Dobric, De Luca, Seow, Selemidis, Bozinovski and Vlahos. This is an open-access article distributed under the terms of the Creative Commons Attribution License (CC BY). The use, distribution or reproduction in other forums is permitted, provided the original author(s) and the copyright owner(s) are credited and that the original publication in this journal is cited, in accordance with accepted academic practice. No use, distribution or reproduction is permitted which does not comply with these terms.

## GLOSSARY

- 4E-BP1** eukaryotic translation initiation factor 4E-binding protein 1
- AEC** animal ethics committee
- AECOPD** acute exacerbation of chronic obstructive pulmonary disease
- ANOVA** analysis of variance
- BALF** bronchoalveolar lavage fluid
- BiP** binding immunoglobulin protein
- CM** conditioned medium
- COPD** chronic obstructive pulmonary disease
- CS** cigarette smoke
- CSA** cross-sectional area
- CSE** cigarette smoke extract
- eIF2 $\alpha$**  eukaryotic initiation factor 2 $\alpha$
- GM-CSF** granulocyte-macrophage colony-stimulating factor
- Gpx1** glutathione peroxidase 1
- IAV** influenza A virus
- IFN- $\beta$**  (*Ifnb*) interferon  $\beta$
- IFN- $\gamma$**  interferon  $\gamma$
- IL-6** interleukin 6
- IL-8** interleukin 8
- JNK** c-Jun N-terminal kinase
- MAFbx** muscle-specific F-box
- Mstn** myostatin
- MuRF-1** muscle RING-finger protein 1
- Myh7** myosin heavy chain 7
- Myog** myogenin
- Nox2** NADPH oxidase 2
- O.C.T** optimum cutting temperature
- PBS** phosphate-buffered saline
- PFU** plaque forming units
- PolyI:C** polyinosinic:polycytidylic acid
- STAT1** signal transducer and activator of transcription 1
- TA** tibialis anterior
- TLR3** toll-like receptor 3
- TNF- $\alpha$**  tumour Necrosis Factor  $\alpha$
- Tpm3** tropomyosin 3